# Fiber Orientation Mapping using Gradient Echo MRI: $R_2$* mapping vs Frequency Difference Mapping

Samuel James Wharton[1], and Richard Bowtell[1]

[1]*Sir Peter Mansfield Magnetic Resonance Centre, School of Physics and Astronomy, University of Nottingham, Nottingham, United Kingdom*

**Introduction:** Fiber orientation mapping through diffusion tensor imaging (DTI) is a powerful technique for visualising white matter (WM) microstructure in the brain [1]. Although DTI provides a robust way to measure fiber orientation, it has some limitations linked to the use of EPI read-outs and long diffusion encoding periods, including relatively low spatial resolution, sensitivity to distortions due to field inhomogeneity and eddy currents, and reduced sensitivity at high field due to $T_2$ and $T_2$* shortening. Development of alternative MRI-based methods for fiber orientation mapping is therefore valuable, in part to allow validation of DTI results. Recently, Lee et al. [2] showed that high-resolution maps of fiber orientation projected into 2D space could be created from gradient echo (GE) images of tissue samples by exploiting the dependence of $R_2$* on the angle, $\theta$, between the fiber axis and $B_0$. Phase data acquired using GE techniques has also been shown to exhibit a dependence on WM fiber orientation [3]. However, non-local effects due to large length-scale field inhomogeneity and macroscopic variation in magnetic susceptibility confound the measurement of phase offsets linked to local microstructure. Sophisticated deconvolution techniques have been developed with the aim of creating locally sensitive phase information, but these can suffer from noise amplification due to the ill-posed nature of the deconvolution [4]. This problem was overcome in recent work by Schweser et al. [5] who showed that frequency difference mapping provides phase-related information that is sensitive to local microstructure. Here, we show that high-resolution 3D fiber orientation maps can be produced from frequency difference or $R_2$* maps acquired with the sample at multiple orientations to the field. This approach was tested on post-mortem brain samples by comparing the resulting orientation maps to DTI data.

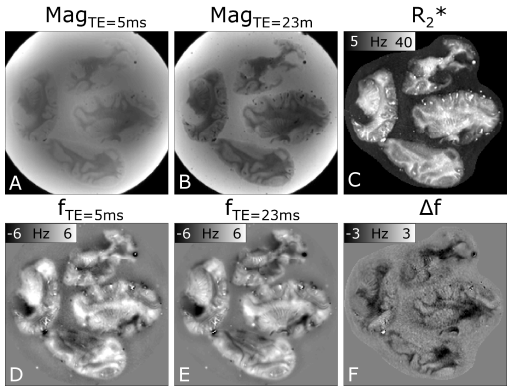


***Fig. 1** Multi-echo magnitude (A&B) and frequency maps (D&E) used to create $R_2$* map(C) and FDM (D).*

**Methods:** Four hemispheres from two non-fixed, adult pig brains (taken from animals sacrificed approximately 24 hours before scanning) were placed inside a spherical, 16cm-diameter Perspex phantom and surrounded by agarose gel. The spherical sample was imaged at 7 T using a multi-echo, spoiled 3D GE sequence (FOV = 170x170x160mm$^3$, isotropic resolution 0.7mm; TR = 30ms, scan time = 25mins). Two echoes with TE = 5 and 23 ms were acquired. The sample was imaged at 16 different orientations incorporating rotations of up to 90$^o$ around the axes perpendicular to $B_0$. At each orientation, $R_2$* maps (Fig. 1C) were created by voxel-wise fitting to the magnitude data (Fig. 1A&B). Frequency difference maps (FDMs) were also produced by: (i) unwrapping and scaling the phase data from each echo by TE, followed by application of weak high-pass filtering, so as to create frequency maps (Fig. 1D&E); (ii) forming a map of the frequency difference, $\Delta f = f_{TE=23ms} - f_{TE=5ms}$ (Fig. 1F). Non-zero intensity in the FDM indicates an area where the phase has evolved non-linearly with TE. As is evident from Fig. 1F non-linear phase evolution occurs predominantly in WM, most likely originating from the rapid decay and orientation-dependent frequency offset of the myelin water signal from WM [5]. DTI data were acquired at 3 T from the spherical sample with isotropic 1.3mm resolution, using 32 diffusion gradient directions. All data were co-registered to the GE images acquired at the first orientation. The dependence of $R_2$* and $\Delta f$ on fiber orientation with respect to the $B_0$-field, was evaluated by pooling the data from all 16 orientations and plotting the values against the angle, $\theta$, between the principle fiber axis (extracted from the DTI data) and $B_0$ (Fig. 2). Only voxels with a fractional anisotropy (FA) > 0.25 were included in this evaluation. Empirical fits (dashed lines in Fig. 2) to the data yielded, $R_2$* = 29 - 2.5cos2$\theta$ + 0.4cos4$\theta$ s$^{-1}$ and $\Delta f$ = -0.5 + 0.8cos2$\theta$ Hz. These fits and the plots in Fig. 2 indicate that $\Delta f$ varies approximately from 0.3 Hz for fibers parallel to the field to -1.3 Hz for perpendicular fibers, while $R_2^*$ is larger by 2.5 s$^{-1}$ for perpendicular versus parallel fibers. By comparing the $R_2$* and $\Delta f$ values for each orientation to the fitted $\theta$-dependencies on a voxel-by-voxel basis it was then possible to carry out a non-linear fit in order to find two parameters for each data-set: (i) the amplitude of the change in $R_2$* and $\Delta f$ with orientation ($A_{R2*}$ and $A_{\Delta f}$); (ii) the fiber orientation expressed as unit vectors $\mathbf{V}_{R2*}$ and $\mathbf{V}_{\Delta f}$ for $R_2$* and $\Delta f$, respectively.

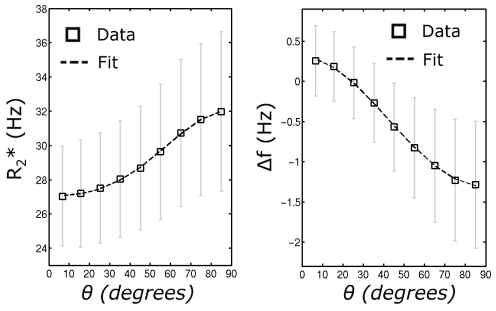


***Fig. 2** θ-dependency curves for $R_2$* and $\Delta f$.*

**Results:** Figure 3 shows maps of the fitted amplitudes (B&C) and colour-coded fiber orientation vectors (E&F) produced from the $R_2$* and $\Delta f$ data. For comparison, the DTI-based FA and fiber-orientation maps are shown in Fig. 3A&D. Correspondence of colours in the maps indicates broad agreement of the fiber orientations identified using the three methods. Further, we evaluated the mean value over WM voxels of the angle between $\mathbf{V}_{DTI}$ and $\mathbf{V}_{\Delta f}$ and between $\mathbf{V}_{DTI}$ and $\mathbf{V}_{R2*}$ finding values of 15$^o$ and 16$^o$, respectively (uncorrelated orientation vectors would yield an angular error of ~ 60$^o$). In addition, the amplitudes, $A_{R2*}$ and $A_{\Delta f}$, are strongly correlated to the fractional anisotropy with correlation coefficients of 0.49 and 0.42, respectively, and associated p-values < 0.0001 in both cases. There are some differences between the $R_2$*- and FDM-based orientation maps, with the latter displaying a generally higher information content.

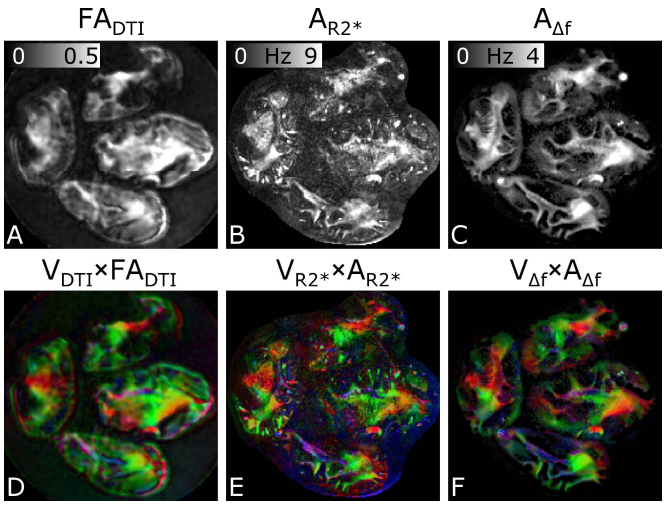


***Fig. 3** DTI-based FA (A) and fiber-orientation map (D). $R_2$* (B&E) and FDM (C&F ) based amplitude (B&C) and fiber-orientation maps (E&F).*

**Discussion:** The results show that there is sufficient fiber-orientation related contrast in 7 T phase and magnitude GE images to produce 3D fiber orientation maps in tissue samples, similar to those produced using DTI. The $R_2$*-based maps are of similar quality to the high-resolution 2D orientation data previously produced from fixed post mortem tissue via $R_2$* mapping at 7T [2]. To our knowledge, Fig. 3F is is the first example of the use of the phase-based information in FDMs to create DTI-like fiber orientation maps. Figure 2 shows that the change in $\Delta f$ with orientation scaled by the uncertainty in $\Delta f$ is significantly larger than the corresponding measure for $R_2^*$, probably explaining the higher quality of the FDM-based orientation maps. This suggests that it may be advantageous in future to use FDM at high field for high resolution fiber-orientation mapping.

**References:** [1] Bihan et al. JMRI. 2001. (13) 534-546; [2] Lee et al. Neuroimage. 2011. (57) 225-234; [3] Lee et al. PNAS. 2010. (107) 5130-5135; [4] Liu et al. MRM. (63) 1471-1477; [5] Schweser et al. Proc ISMRM. 2011. 1428.